Clays and Clay Minerals, Vol. 49, No. 4, 355–369, 2001.

MINERALOGY, GEOCHEMISTRY AND UTILIZATION STUDY OF THE MADAYI KAOLIN DEPOSIT, NORTH KERALA, INDIA

C.S. MANJU[1], V. NARAYANAN NAIR[2] AND M. LALITHAMBIKA[1]

[1]Regional Research Laboratory (CSIR), Industrial Estate P.O., Thiruvananthapuram 695019, Kerala, India
[2]Department of Geology, University of Kerala, Thiruvananthapuram, Kerala, India

Abstract—The Madayi clay deposit consists of a thick sequence of residual white kaolinitic clay underlying the sedimentary Warkallai Formation, which includes gray carbonaceous kaolinitic clays, lignite, ferruginous kaolinitic clays, laterite and bauxite with ferricretes. The conditions of clay genesis and the economic significance of the major residual kaolin seam have been investigated. The raw clay and <2 μm fractions were subjected to X-ray diffraction (XRD), chemical analysis, differential thermal analysis (DTA), Fourier transform infrared (FTIR) spectroscopic and scanning electron microscopic (SEM) studies. The firing behavior of the <45 μm fraction of the major residual clay sequence (L), was investigated systematically to determine the potential industrial use of this kaolin.

Geochemical and morphological studies of different strata indicate the following conditions for clay formation: (1) intense lateritized weathering conditions for kaolinization of the residual white clay from parent quartzo-felspathic mica-gneiss; (2) reducing environment for the gray carbonaceous layers; and (3) oxidizing environment for the uppermost hematite-rich ferruginous clay. Pyrite/marcasite enriched detrital gray carbonaceous clay shows two distinct environments for *in situ* kaolinite crystallization: (1) within plant fossils influenced by the high organic content and FeS_2 leaching; and (2) precipitation from solution.

Incomplete kaolinization of white residual clay is evident from the presence of pyrophyllite, muscovite with lenticular cleavage void and a lower percentage of fines (<2 μm). The plant fossils from the uppermost portion of residual clay show pyrite mineralization. The Hinckley Index, FTIR and rare earth analysis point towards diverse geochemical environments of deposition and technological evaluation indicates its suitability for application in the ceramics industry.

Key Words—Genetic Environment, Gray Carbonaceous Clay, Hematite-Rich Clay, Madayi, Morphology, Recrystallization, Residual Kaolinite, Technological Evaluation, Trace Elements.

INTRODUCTION

Kaolinitic clays are geochemically and industrially very versatile. The majority of the known clay deposits in the southern part of the Indian Peninsula are of sedimentary or residual origin. These kaolinitic clays formed under tropical weathering conditions characterized by alternate wet and dry seasons with high humidity and moderately high temperatures. These conditions with periodic rainfall promote rapid chemical break up of the parent material. A systematic study was carried out to show the variations in chemistry, structure and morphology of kaolinite collected from the deposit at Madayi village, (75°15′00″–75°16″00″E; 12°01′45″–12°02′30″N) (Figure 1A) in Kannur district, Northern Kerala. The analysis, by various techniques, of clays collected from different layers gives a detailed picture of the mineralogical assemblages and the nature of the mineral species. An attempt was made to define the process that leads to the formation of the genetically different varieties of kaolinite within the same deposit by characterizing different clay layers (Figure 1C). Laboratory tests were also conducted to identify possible uses of the china clay seam L (Figure 1C), which is industrially viable, having a reserve of ~17 million tonnes within an area of 1.2 sq. km.

GEOLOGICAL SETTING

Geologically, the area consists of Precambrian crystalline rock overlain unconformably by a thick sequence of the Warkallai Formation of Miocene age. Thick deposits of residual and sedimentary clay sequences, having an overall thickness of 45 m are associated with these. This clay deposit is confined to the southern part of the Tertiary sedimentary basin, which extends from Kannur to Kasargod.The extent of the different types of clays in this location was identified by the Department of Mining and Geology, Kerala (internal report, 1995) (Figure 1B). Since it was found to be a potentially viable deposit, detailed investigation was undertaken.

The sedimentary clays of this region belong to the Warkallai Formation of Miocene age which is characterized by a thin layer of sand, alternate layers of carbonaceous clays and lignite seams followed by Fe-rich variegated clay, laterite and bauxite with ferricretes at the top (Figure 1C). The topmost clay layer L16 is a strong red colour and is ~0.6 m thick. The carbonaceous clay layers, L15, L13, L11, L9, L7, L5 and L3 alternate with lignite seams L14, L12, L10, L8, L6, L4 and L2 forming an overall thickness of ~17.5 m. The upper two carbonaceous clay seams L15 and L13 show mottled reddish yellow patches. Black colored patches can be seen within the lower L9, L7 and L3

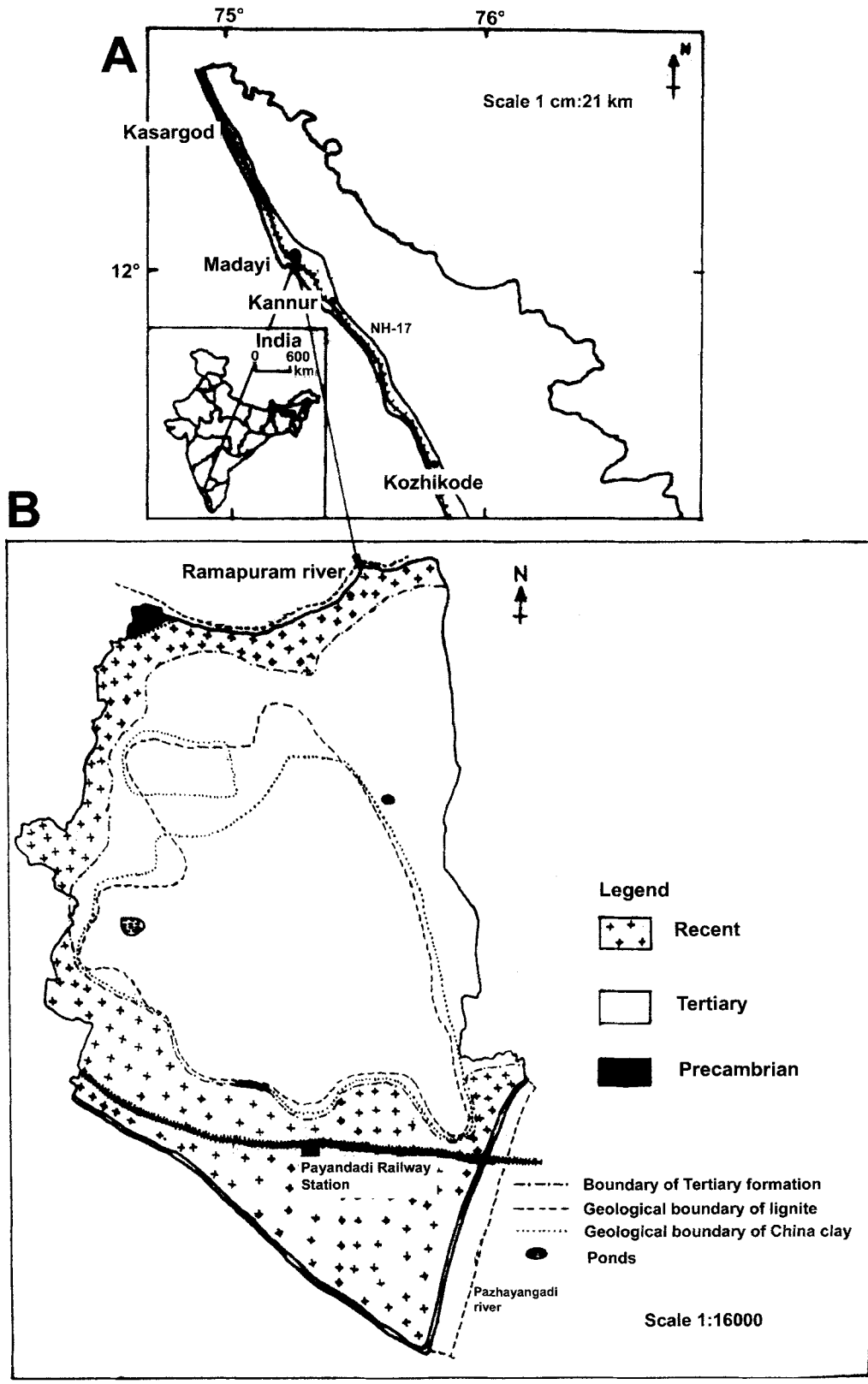

Figure. 1. (A) Schematic representation of the area under study; (B) geological map of Madayi; (C) schematic cross-section of Madayi deposit.

https://doi.org/10.1346/CCMN.2001.0490409 Published online by Cambridge University Press

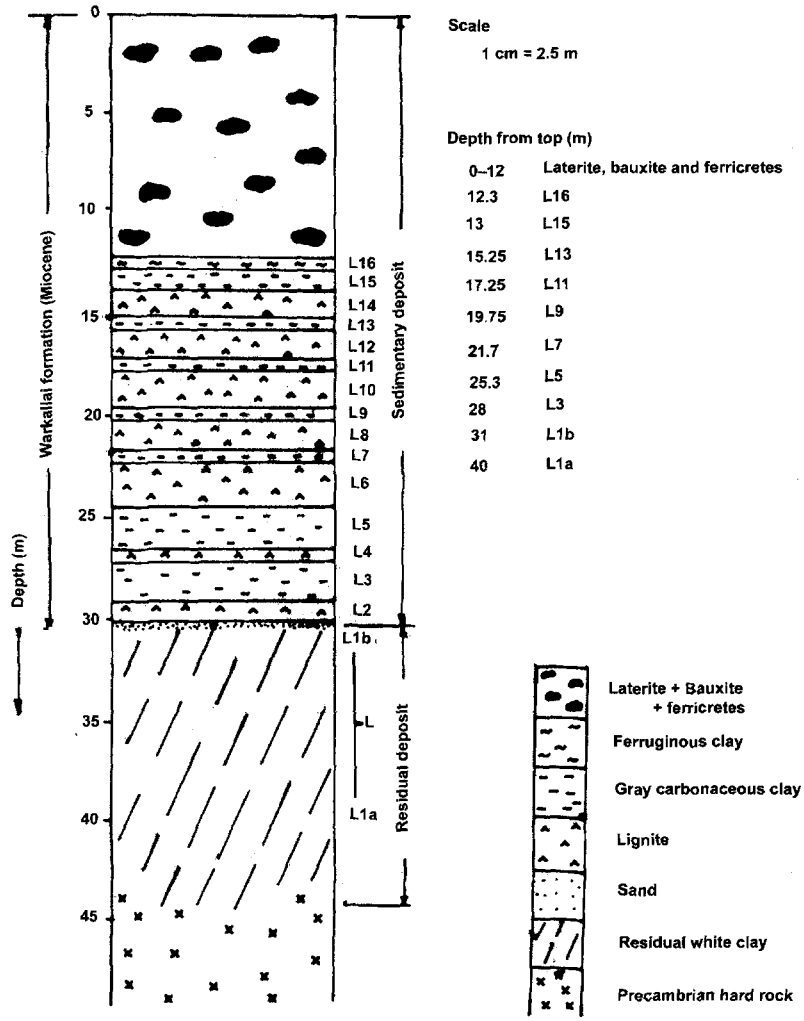

Figure. 1. Continued.

clay seams. Ample fossilized plant remains were found both in the carbonaceous clay and lignite seams. The entire sedimentary deposit is ~30 m thick and is underlain by residual white clay. A thin veneer of sand separates the overlying sedimentary and the underlying residual clay.

The residual white clay L (L1a and L1b) which is approximately 10–15 m thick (Figure 1C), has relict structures like foliation and intruded quartz veins inherent from the parent rock, a quartzo-feldspathic mica-gneiss of Precambrian age. Numerous fossilized plant roots, ~0.1–0.35 m from the top of the residual clay L, were identified during field excavation. This shows evidence of plant growth and subsequent weathering prior to Tertiary sedimentation. Field evidence and detailed geological studies of the regions around North Kerala by Rajendran and Narayanaswamy (1987) indicate the influence of two spells of lateritization, *i.e.* pre-Warkallai and post-Warkallai-pre-Quaternary lateritization on the country rock. The pre-Warkallai lateritization resulted in the formation of the thick white residual clay. In addition, weathering after the deposition of the Warkallai Formation resulted in thick deposits of laterites and bauxite which overlie the gray carbonaceous clay seams.

MATERIALS AND METHODS

Representative clay samples were collected from each of the recognizable layers (Figure 1C). Sampled materials were crushed in an agate mortar and a fraction of the raw clay was used for mineralogical and chemical analysis. The <2 μm clay fraction separated by sedimentation and centrifugation was analyzed for clay minerals and associated impurities by oriented XRD and DTA. Structural characterization of the <2 μm fraction of kaolinite was carried out by FTIR spectroscopy and determination of the Hinckley crystallinity index (Hinckley, 1963), after the removal of

https://doi.org/10.1346/CCMN.2001.0490409 Published online by Cambridge University Press

Table 1. Semi-quantitative mineralogical analysis by XRD (raw clay and <2 μm fraction).

Sample	K	Sm	M	Py	I	G	Q	P	Ma	H	A
Raw clay:											
L1a	****		***	***	**	**	****				
L1b	****		***	***	**	**	****				
L3	****					***	****	***	***		**
L5	****					***					
L7	****					***	****	***	***		**
L9	****					***	****	***	***		
L11	****					***	****	***	***		
L13	****						****	**	**		
L15	****							***	***		
L16	****						**			****	
<2 μm											
L1a	****				***	**	**				
L1b	****				***	**	**				
L3	****					***	***	***	***		
L5	****	**				***					
L7	****					***	****	***	***		
L9	****						****	***	***		
L11	****					***					
L13	****							**	**		
L15	****						***	**	**		
L16	****									***	

K—kaolinite, Sm—smectite, M—muscovite, Py—pyrophyllite, I—illite, G—gibbsite, Q—quartz, P—pyrite, Ma—marcasite, H—hematite, A—anatase. The symbols in the table represent: **** major phase, *** minor phase, ** trace phase.

carbonate by sodium acetate, iron oxides by citrate-bicarbonate, and organic matter by H_2O_2 (Al-Khalissi and Worrall, 1982).

The XRD analysis was performed using Ni-filtered CuKα radiation (40kV, 20 mA) at a scan speed of 1° 2θ/min. The DTA was carried out using a Seiko 320 TG/DTA analyzer at a heating rate of 10°C/min from ambient temperatures to 1100°C with alumina as standard. The FTIR spectra of 1 mg of the pretreated fraction, mixed and pelletized with 200 mg of KBr, were recorded over the range of 4000–400 cm^{-1} using a Perkin Elmer IR Spectrometer after overnight drying at 60°C.

The pH of the raw clay samples was measured using 1:4 solid water ratios. Organic carbon in these samples was determined by oxidative decomposition using $K_2Cr_2O_7$ as the oxidizing agent (Gross, 1971). The concentration of pyritic and non-pyritic iron was determined by the acid dissolution technique (Schneider and Schneider, 1990). The raw clay and the <2 μm fraction were analyzed for SiO_2, Al_2O_3, Fe_2O_3, TiO_2, K_2O, CaO, Na_2O, MgO and LOI (Bennett and Reed, 1971). The trace element analysis of three selected raw samples (L1a, L7 and L16) was carried out by ICP-MS. Scanning electron microscopic analysis of raw clay and hand-picked plant remains was performed using a JEOL JSM 5600 LV microscope. Freshly broken natural surfaces of the specimens were sputter coated with gold prior to the analysis.

Laboratory tests were conducted using the <45 μm fraction of residual china clay L, an economically viable belt within the Madayi deposit. The physical properties and firing behavior were tested in order to evaluate their utilization in the ceramic industry. Grain-size analysis of the <45 μm fraction was carried out by Micromeritics Sedigraph 5100 using calgon as the dispersant. Viscosity measurement of 63% w/w slurry was undertaken with a Brookfield viscometer using minimum concentration of sodium polysalt as a dispersing agent. Crude and calcined samples (350°C, 1 h) (Kogel and Hall, 1999) were bleached increasingly with 0.4% sodium hydrosulfite for brightness improvement. This was measured using a Color Touch Model ISO brightness meter. Brightness was measured on dried samples (100°C, 1 h) at 457 nm and the yellowness as a difference in brightness between 570 and 457 nm. The water of plasticity, green MOR, fired MOR (1250°C) and linear shrinkage (dry and fired (1250°C)), were measured as specified in ASTM standards. Volume shrinkage, bulk density, water absorption and apparent porosity (ASTM) of the samples were analyzed by firing the samples at temperatures of 600, 800, 1000 and 1250°C (1 h soaking). The fired color of the sintered samples was also noted.

RESULTS AND DISCUSSION

XRD studies

The mineralogical analyses of raw clay and the <2 μm fraction are summarized in Table 1. The constituent minerals were expressed as major, minor and

trace depending on their concentrations. The residual clays, L1a and L1b, consist chiefly of kaolinite and quartz with considerable muscovite, gibbsite and pyrophyllite (Figure 2A). The <2 μm clay fraction (Figure 2B) is devoid of pyrophyllite, suggesting its conversion to kaolinite. The same conclusion was reported by Heckroodt and Buhmann (1987) suggesting the formation of pyrophyllite from muscovite during early stages of weathering and its alteration to kaolinite at a later stage. Microcrystalline quartz and fine-grained mica, *i.e.* illite, constitute minor ingredients.

Most of the gray carbonaceous clays, except L5, exhibit an association of pyrite and marcasite along with kaolinite, quartz and gibbsite. Sedimentary pyrite formation occurs during the reaction of a detrital iron mineral with H_2S, which was formed by the reduction of sulfate by bacteria in the presence of organic matter (Berner, 1984). The small shoulder at 3.52 Å in the XRD patterns (Figure 2A) of L3 and L7 indicates anatase. Trace amounts of smectite were identified in L5 (14 Å) (Figure 2B). The formation of smectite is favored by a microenvironment with poor drainage and hence minimum leaching conditions with relatively high metal ion concentrations (Keller, 1985). Gibbsite identified by the 4.84 Å peak in L3, L5, L7, L9 and L11 indicates intense leaching in a strongly deionized environment under tropical climate (Vazquez, 1981) during desilication, *i.e.* dissolution of Si from its aluminosilicate parent material. From the available information it is not clear whether the gibbsite found in these carbonaceous clay is the product of post or predepositional alteration. The association of the above minerals in the same clay resulted from the changes in the microenvironment during the clay deposition or formation. Fine quartz grains (<2 μm) were noted in the carbonaceous clays having large amounts of marcasite/pyrite (evident from peak intensity, Figure 2B). Chen *et al.* (1997) suggest formation of microcrystalline quartz as a result of the rearrangement of the feldspar and muscovite structures during kaolinization or kaolinite recrystallization.

The ferruginous L16 clay shows an assemblage of kaolinite, quartz and hematite. Hematite is concentrated in the fine clay fraction. The presence of hematite indicates an oxidizing environment and the presence of Fe sulfides indicates reducing environment conditions during the formation or deposition of gray carbonaceous and ferruginous clay, respectively.

The Hinckley crystallinity index of kaolinite varies from clay layer to clay layer (Table 2). This variability may be attributed to differences in the geological environment such as intensity of weathering or the extent of transportation of the clay during formation or deposition (Brindley, 1986). The crystallinity index varies from 0.44 (L5) to 0.86 (L1a).

Chemical analyses

The chemical analysis and pH values of the samples are listed in Table 2. The SiO_2 and Al_2O_3 contents of L1a and L1b were consistent with mineralogical observation. The relatively lower K_2O concentration in L1b compared to L1a from the same seam at a difference in depth of 10 m indicates its preferential leaching from muscovite.

The major oxide in gray carbonaceous clay, SiO_2, is present in lower concentrations than in the residual clays above. This might be due to the winnowing action during transportation and sedimentation. Lack of a particular trend in the TiO_2 distribution with depth, indicates its immobile nature during weathering. The MgO concentrated in the <2 μm fine fraction is attributed to smectite. High Fe_2O_3 accounts for the presence of FeS_2 minerals, marcasite and pyrite (Table 2). Hematite contributes to the major source of iron in ferruginous clay and the maximum iron content of this deposit is found in this clay fraction (22.20%) (Table 2).

The pH of the clays ranges from 2.64 to 5.48. The high acidity implies the effect of ongoing weathering. The acidity correlates with the FeS_2 and organic carbon content. The pH is lowest in L3 (2.64) where organic carbon (7.23%) and FeS_2 (9.96%) are relatively high. The FeS_2 is highly concentrated in L9 (15.37%), L7 (8.47%) and L3 (9.96%) where the carbon content and Fe_2O_3 are also high.

The distribution of trace elements in L1a, L7 and L16 (Figure 3) shows some variation. Vanadium (V^{4+}) is more concentrated in the hematite-rich clay in the presence of relatively high TiO_2 and Fe_2O_3 (Table 2). Vanadium (V^{4+}) with an ionic radius of 0.61 Å replaces Ti^{4+}(0.64 Å) (Rankama and Sahama, 1952) and also precipitates in ferric hydroxides (Goldschmidt, 1958). Zirconium, almost entirely contained in the mineral zircon, is found to be concentrated more in the hematite-rich sedimentary clay (180 ppm), followed by the gray carbonaceous clay (118 ppm), suggesting concentration during the course of weathering, transportation and deposition. Manganese shows similar ranges in concentration. The Cu can be correlated with Zn; where an increase in the concentration of Cu occurs, the Zn content also increases. The total trace element concentrations for L1a, L7 and L16 are 498.71, 837.61 and 881.69 ppm, respectively.

DTA studies

The DTA patterns (<2 μm) (Figure 4) show features related to the mineralogical assemblage and the kaolinite structure. The dehydroxylation and exothermic peaks of kaolinite range from 522 to 542°C and 972 to 1000°C, respectively. Higher exothermic temperatures for kaolinite were noted in L1a (1000.9°C) and L1b (1003°C) and lower peak temperatures were

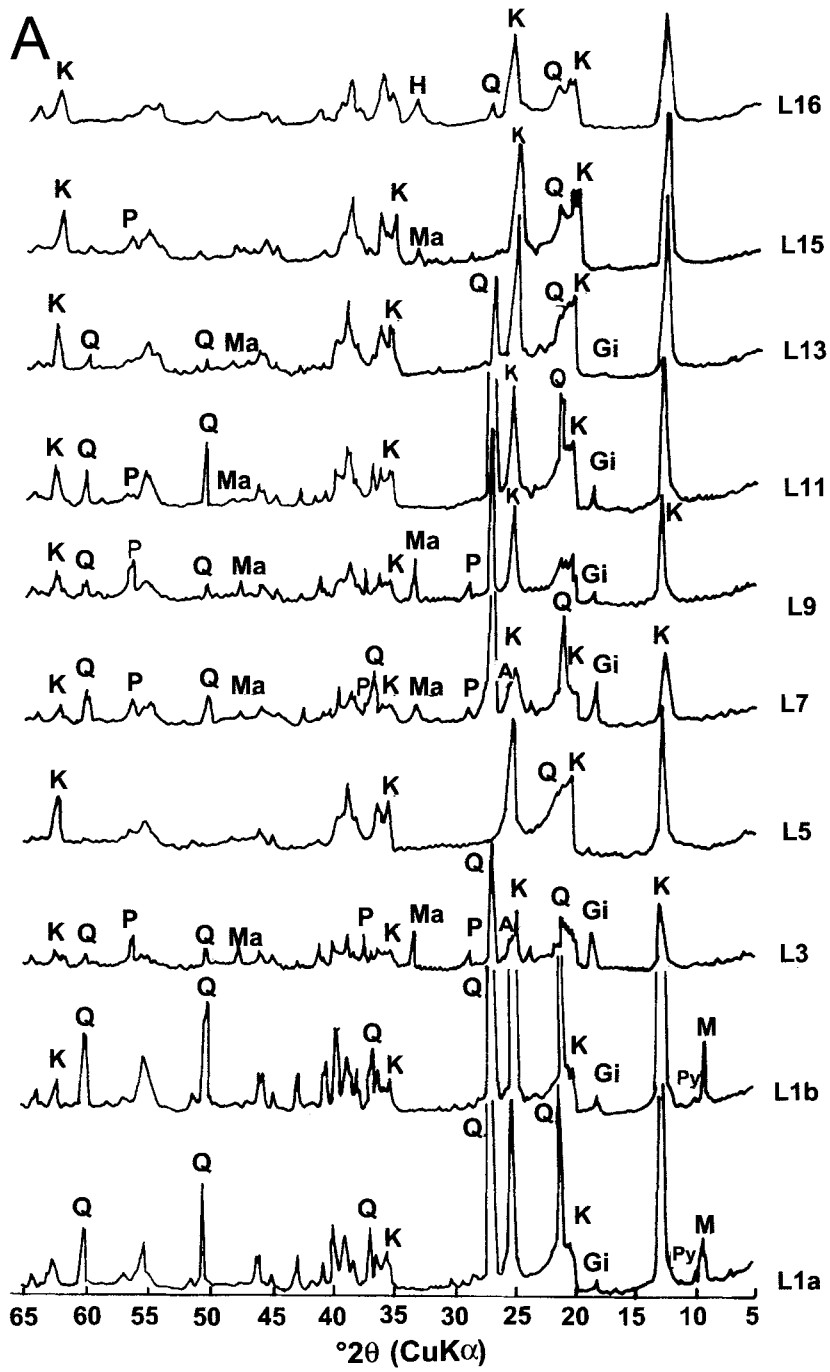

Figure 2. (A) XRD pattern of raw clay samples: L1a and L1b—the lowermost residual clay layer; L3, L5, L7, L9, L11, L13, L15—the carbonaceous gray clay with decreasing order of depth from the top; and L16—ferruginous clay. K—Kaolinite, Py—Pyrophyllite, Gi—Gibbsite, Q—Quartz, P—Pyrite, Ma—Marcasite, M—Muscovite, H—Hematite, A—Anatase. (B) XRD pattern of oriented <2 μm clay fraction: L1a and L1b—the lowermost residual clay layer; L3, L5, L7, L9, L11, L13, L15—the carbonaceous gray clay with decreasing order of depth from the top; and L16—ferruginous clay. K—Kaolinite, Gi—Gibbsite, Sm—smectite, Q—Quartz, P—Pyrite, Ma—Marcasite, I—illite, H—Hematite, A—Anatase.

https://doi.org/10.1346/CCMN.2001.0490409 Published online by Cambridge University Press

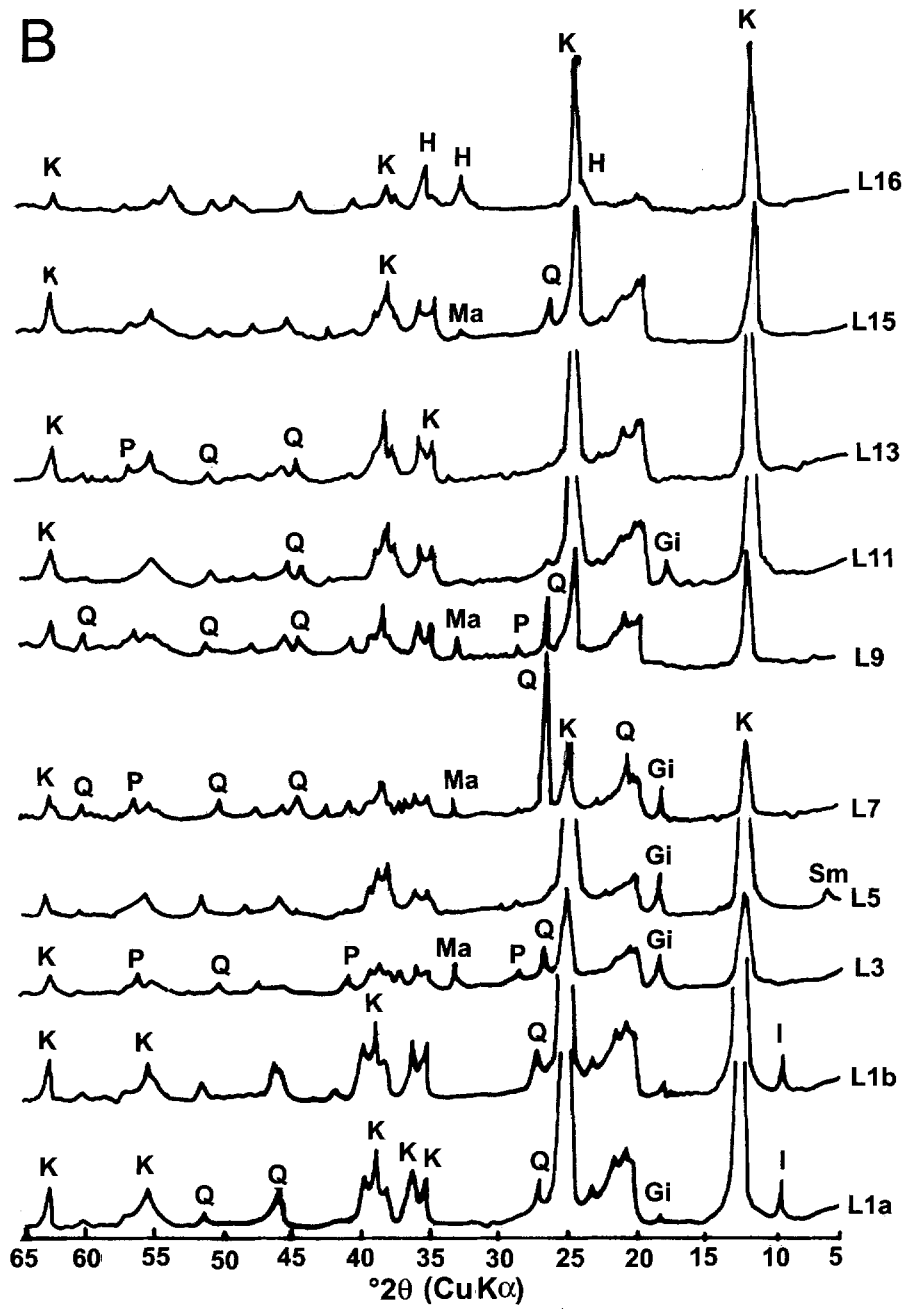

Figure. 2. Continued.

noted in the gray carbonaceous clays. The exothermic peak typical of kaolinite, showing the formation of a new phase, mullite, is not prominent in L3, L7 and L9 where there is a higher concentration of pyrite. This mineral may act as flux, which affects the thermal property. An additional peak at 450°C was also noticed in the above clays, which is characteristic of pyrite (Searle and Grimshaw, 1960). Mineralogical and chemical analysis also supports this evidence. The dehydroxylation temperature at 277–290°C is that of gibbsite.

IR studies

The structural analysis of kaolinite by XRD and DTA was further complemented by detailed FTIR studies. The spectra (Figure 5) give valuable information about the degree of crystallinity and regularity of structure of the clay minerals (Russell,

https://doi.org/10.1346/CCMN.2001.0490409 Published online by Cambridge University Press

Table 2. Chemical analysis of clay samples from different layers (wt. %).

	L1a	L1b	L3	L5	L7	L9	L11	L13	L15	L16
SiO_2	65.03	63.9	34.92	51.07	46.49	35.02	52.60	43.24	37.67	43.47
	45.26	46.02	36.82	38.98	34.06	37.59	38.31	40.38	9.76	28.21
Al_2O_3	21.61	23.91	26.23	26.92	25.45	28.72	27.08	33.69	37.30	29.77
	38.02	36.17	29.20	36.85	34.06	37.01	35.89	36.02	38.06	35.22
Fe_2O_3	1.43	1.27	10.76	1.97	6.64	9.81	1.35	2.36	2.89	11.90
	0.38	0.75	6.82	1.26	5.34	2.87	1.42	1.34	2.68	22.20
TiO_2	0.02	1.30	1.00	0.98	1.44	1.59	1.35	1.84	3.35	1.85
	0.06	0.32	0.10	0.81	2.27	2.86	3.62	2.54	1.05	0.16
Na_2O	0.16	0.12	0.26	0.18	0.29	0.22	0.21	0.17	0.18	0.37
	0.45	0.33	0.45	2.04	0.67	0.53	0.67	0.58	0.98	0.36
K_2O	2.51	1.90	1.05	0.60	2.24	2.24	3.73	1.50	1.20	0.09
	0.65	0.39	0.37	1.83	0.55	0.51	0.49	0.58	0.54	0.58
MgO	0.01	0.33	0.04	0.07	0.01	0.03	0.01	0.05	0.27	0.21
	0.06	0.11	0.13	0.52	0.02	0.15	0.06	0.33	0.40	0.49
CaO	0.10	0.13	0.13	0.28	0.39	0.41	0.18	0.13	0.14	0.38
	0.11	0.13	0.41	0.55	0.42	0.28	0.28	0.13	0.28	0.70
LOI	9.59	9.38	24.49	18.20	17.33	21.62	13.04	17.13	17.13	12.81
	14.41	14.69	25.56	17.04	18.36	17.93	16.02	15.43	16.75	12.08
C#	0.21	0.45	7.23	1.08	3.31	5.84	0.99	0.64	0.73	0.42
FeS_2#	0.18	0.31	9.96	1.15	8.47	15.37	1.34	0.95	1.36	—
pH#	3.99	3.49	2.64	3.14	2.75	2.67	3.29	2.77	2.77	5.48
HI*	0.86	0.69	0.72	0.44	0.70	0.70	0.51	0.64	0.50	0.67

Upper readings relate to raw clay, lower readings to the <2 μm fraction.
#—raw clay, * <2 μm fraction, HI—Hinckley Index, — below detection limit.

1987). The IR spectra show the prominent peaks of kaolinite: 3620–3700 cm^{-1} for –OH stretching, 1000–1120 cm^{-1} for –Si–O stretching, 910–940 cm^{-1} for –OH bending and 400–550 cm^{-1} for –Si–O bending vibrations (Farmer, 1979).The differences in band intensities as evident from the peak height differences, suggest a variety of defects in kaolinite structure. The doublet between 3694 and 3619 cm^{-1} for L1a, L3, L7, L11, L13 and L15 is indicative of well-ordered kaolinite structure (Farmer, 1979; Russell, 1987). A degree of order for the clays above is also clear from the IR band intensities at 791 and 751 cm^{-1}. The relative intensity of these bands is the same for ordered kaolinite and the band at 791 cm^{-1} becomes weak with increasing disorder. The presence of the doublet in the gray carbonaceous clays, which have a lower Hinkley index (Table 2), might be due to the mixture of ordered and disordered kaolinite. The features above could be explained by the order/disorder index proposed by Plançon *et al.* (1989), which measures the relative proportion of high-defect components. The better ordered kaolinites, as evident from FTIR, were formed as a result of the recrystallization of low-order detrital ones. This evidence of recrystallization is reinforced by the SEM studies.

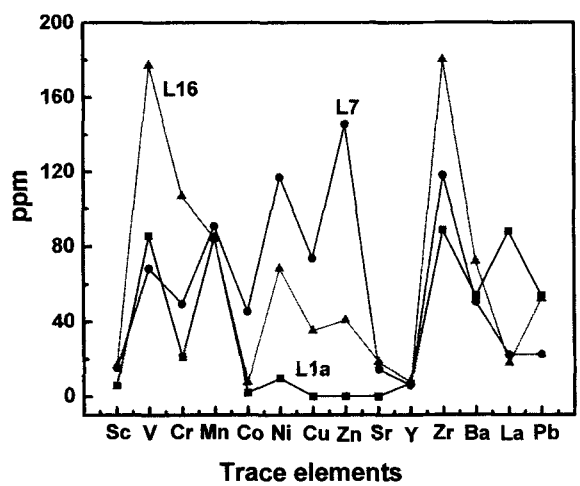

Figure 3. Trace element patterns of three selected raw clay samples, L1a, L7 and L16.

SEM studies

Scanning electron micrographs of clay from L1a, L3, L5, L15, L16 and the fossilized plant remains clearly indicate the geochemical processes and environment for the genesis of three distinct clays in this particular deposit.

Residual white clay. Vermicular and book-like morphology is observed for the residual L1a clay (Figure 6A). Almost all kaolinite grains exhibit a face-to-face pattern of arrangement of platy crystals (Figure 6A). The residual kaolinite shows crystals with angular edges (Figures 6A and 6B), which suggest *in situ* formation. The irregular angular kaolinite edge is characteristic of actively growing crystals (Keller, 1985). Kaolinite grains were found at the edge of micaceous stacks or books suggesting the

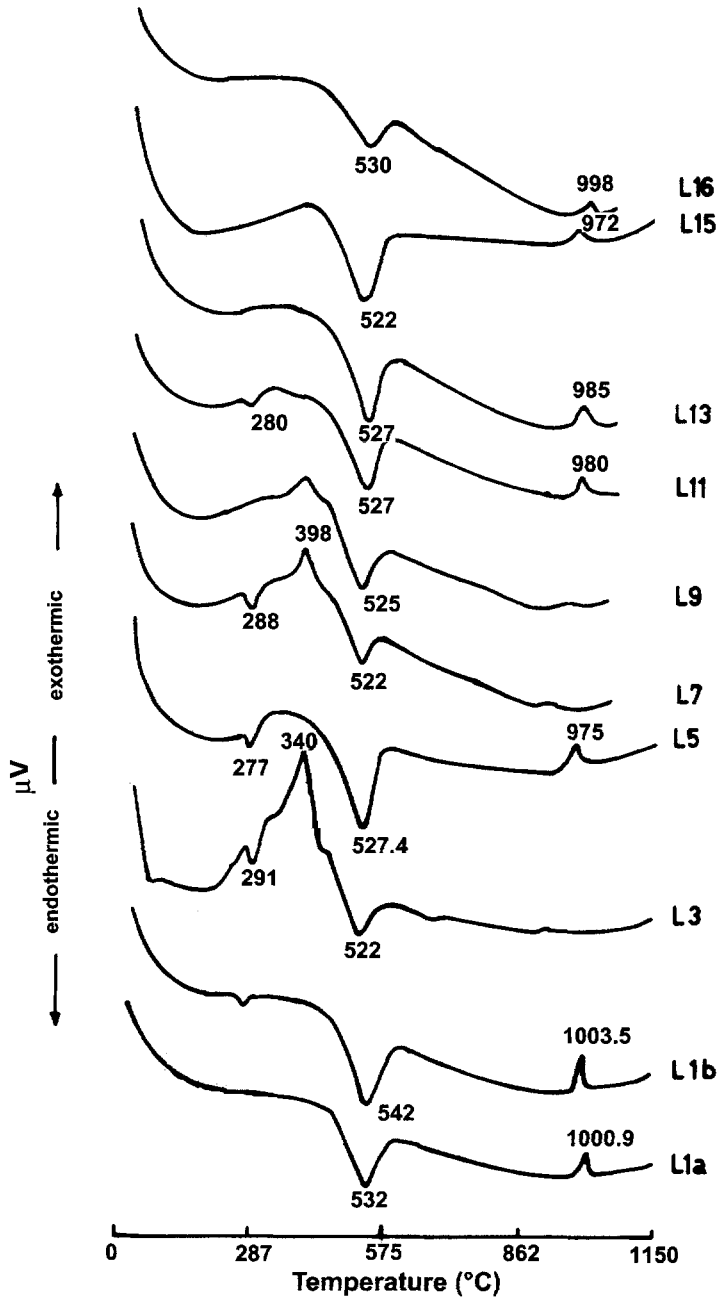

Figure 4. DTA curves of <2 μm fraction showing varying endothermic-exothermic temperature.

alteration of muscovite to kaolinite (Figure 6B). This particular morphology implies the initiation of kaolinization from the edges of the muscovite stacks and weak cleavage planes. The muscovite stacks show a typical fanning out texture, formed by the release of K during hydration or hydrolysis (Stoch and Sikora, 1976; Chen *et al.*, 1997) forming numerous lenticular voids along the cleavage planes. The formation of these lenticular voids during weathering is attributed to the volume decrease during the collapse of the muscovite structure (Robertson and Eggleton, 1991). These lenticular voids indicate an incomplete stage for kaolinization since they disappear during the completion of weathering of the primary phyllosilicates (Robertson and Eggleton, 1991; Chen *et al.*, 1997). Compact tabular muscovite grains (Figure 6C) without any indication of alteration could also be identified. The K-defi-

https://doi.org/10.1346/CCMN.2001.0490409 Published online by Cambridge University Press

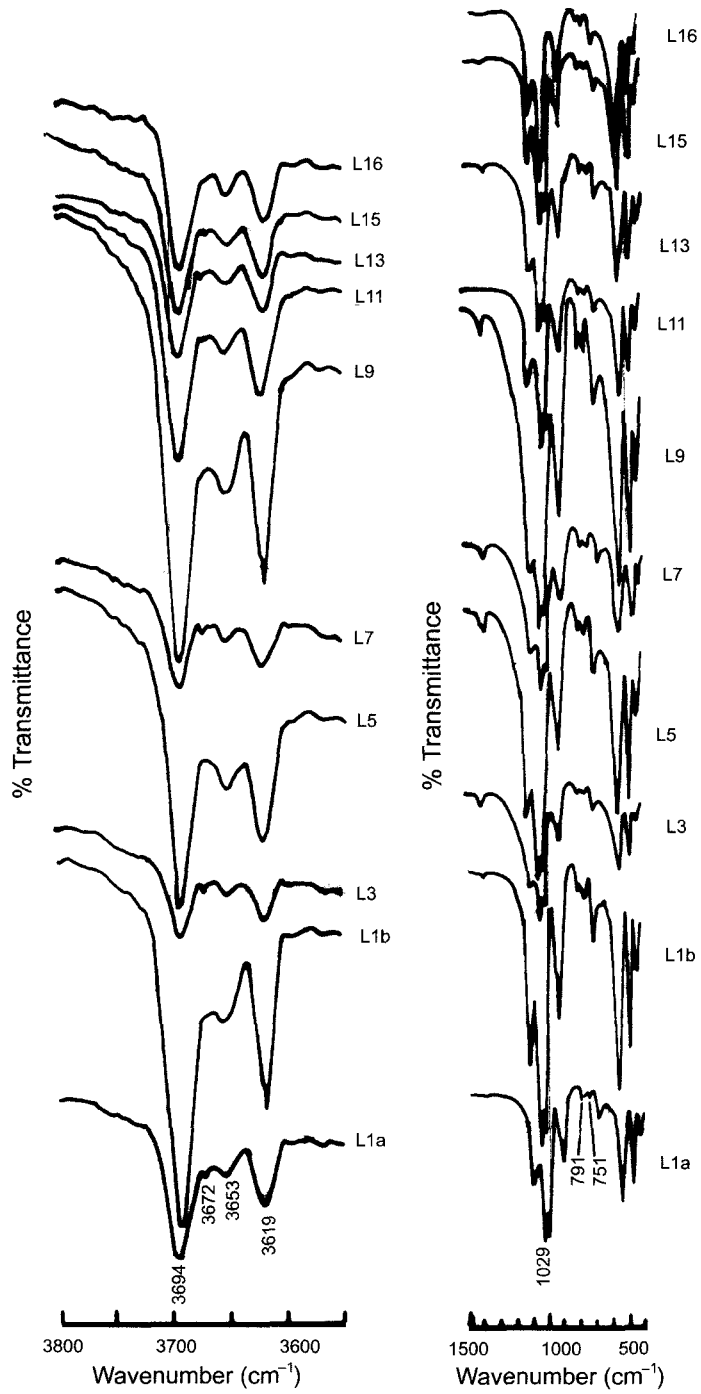

Figure 5. FTIR spectra of <2 μm clay sample (3900–3700 cm^{-1}) (1500–400 cm^{-1}) with weak doublet between 3694 and 3619 cm^{-1} and relative intensities of 791 cm^{-1} and 751 cm^{-1} reflecting the crystalline order of kaolinite.

cient muscovite crystals characteristically had a more irregular shape than the typical prismatic laths of fresh muscovite.

Fossilized plant roots from uppermost residual clay show mineralization. *In situ* pyrite crystals with the morphology of octahedron, pyritohedron, dodecahedron and octahedron-cube combination (Figure 6D) were observed to grow from the sidewall of plant fossils. These particular crystal morphologies are similar to that of pyrite forming from an undersaturated so-

https://doi.org/10.1346/CCMN.2001.0490409 Published online by Cambridge University Press

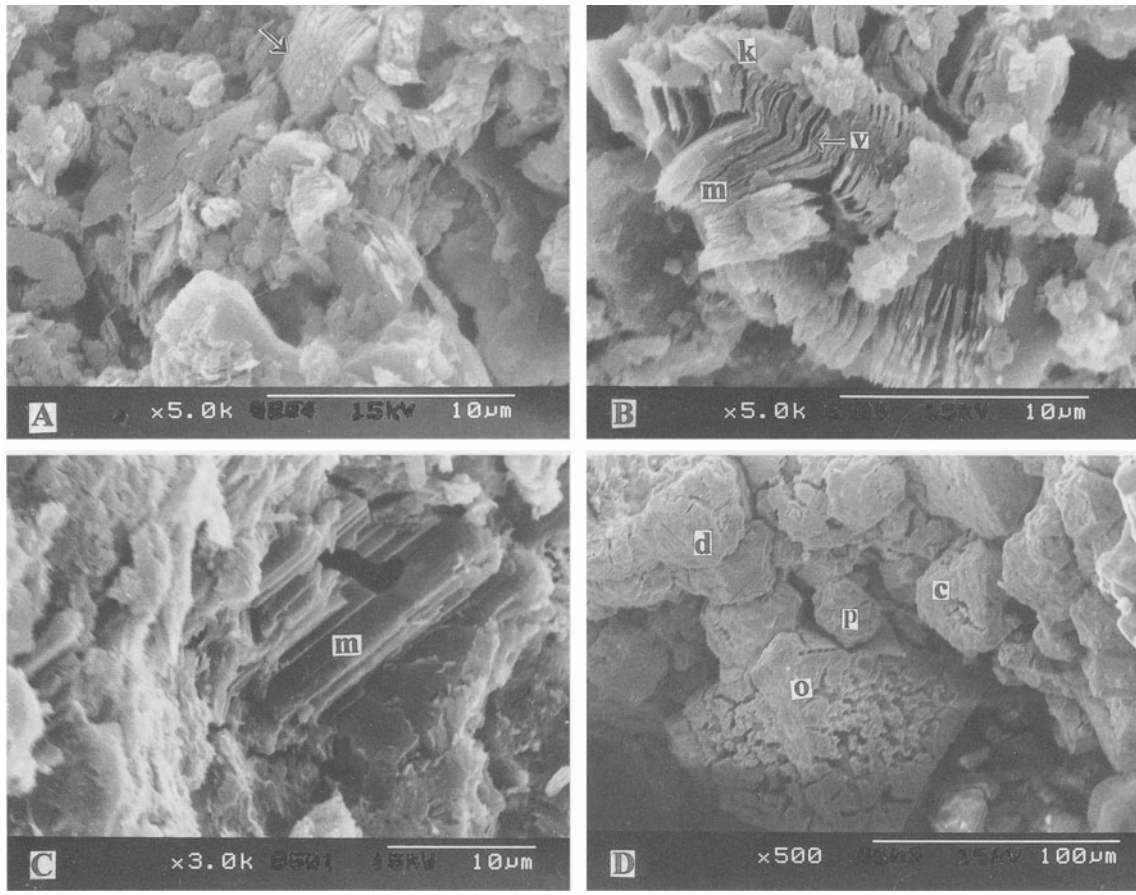

Figure 6. Scanning electron micrographs illustrating residual clay: (A) kaolinite books (arrow), with irregular edges showing *in situ* crystallization and friated appearance, indicative of mica alteration; (B) fanning out of muscovite (m), along with kaolinite (k) at the edges, with numerous lenticular voids (v) between the flakes due to K leaching; (C) muscovite grain (m) without alteration, embedded in the kaolinite platelets; (D) mineralization within hand-picked plant remains from uppermost portion L1b residual clay: *in situ* crystallization of Fe sulfide crystals with o (octahedral), d (dodecahedral), p (pyritohedral), c (cube-octahedral) combination. The grains show etched pits on their surfaces.

lution (White *et al.*, 1991). Numerous etched pits were also found on the surface of the grain (Figure 6D), formed as a result of ongoing weathering, during the percolation of ion-rich solutions. The FeS_2 mineralization in the residual white clay might have resulted from the influence of the leached acid-rich pore-water from the overlying organic and FeS_2-enriched gray carbonaceous clay layers during oxidation.

Sedimentary gray carbonaceous clay. This clay shows two types of kaolinite formation in addition to its detrital character. Clay fraction L5 shows a swirl texture (Figure 7A) with face-to-face arrangement of grains suggesting their detrital origin (Keller, 1978). In the sedimentary clay L15, finer clay grains are agglomerated during their deposition by the cementing effect of organic matter (Figure 7B), thereby giving a flower-like appearance.

The lowermost gray carbonaceous clay (L3) has two types of grains (Figure 7C), suggesting the diversity of the environment for their formation. The smaller kaolinite grains are angular with a typical face-to-face arrangement, surrounding larger hexagonal grains having smooth edges. These bimodal features indicate that the finer grains are a recrystallized product and the coarser grains are of detrital origin. This texture in kaolinite occurs due to *in situ* formation of this particular mineral in a water-laden environment from silicate parent material (Keller, 1978).

The second type of *in situ* kaolinite within gray carbonaceous clay is observed as mineralization within the fossilized plant remains collected from L15 strata. Stacks of kaolinite platelets were found grown into the cubic etched pits formed by the dissolution of the cubic pyrite (Figure 7D), suggesting kaolinite crystallization after the removal of FeS_2 during oxidation. Oxidation of organic matter along with FeS_2 leads to the formation of acid-rich pore-fluid which will disintegrate and dissolve the kaolinite and reprecipitate this

https://doi.org/10.1346/CCMN.2001.0490409 Published online by Cambridge University Press

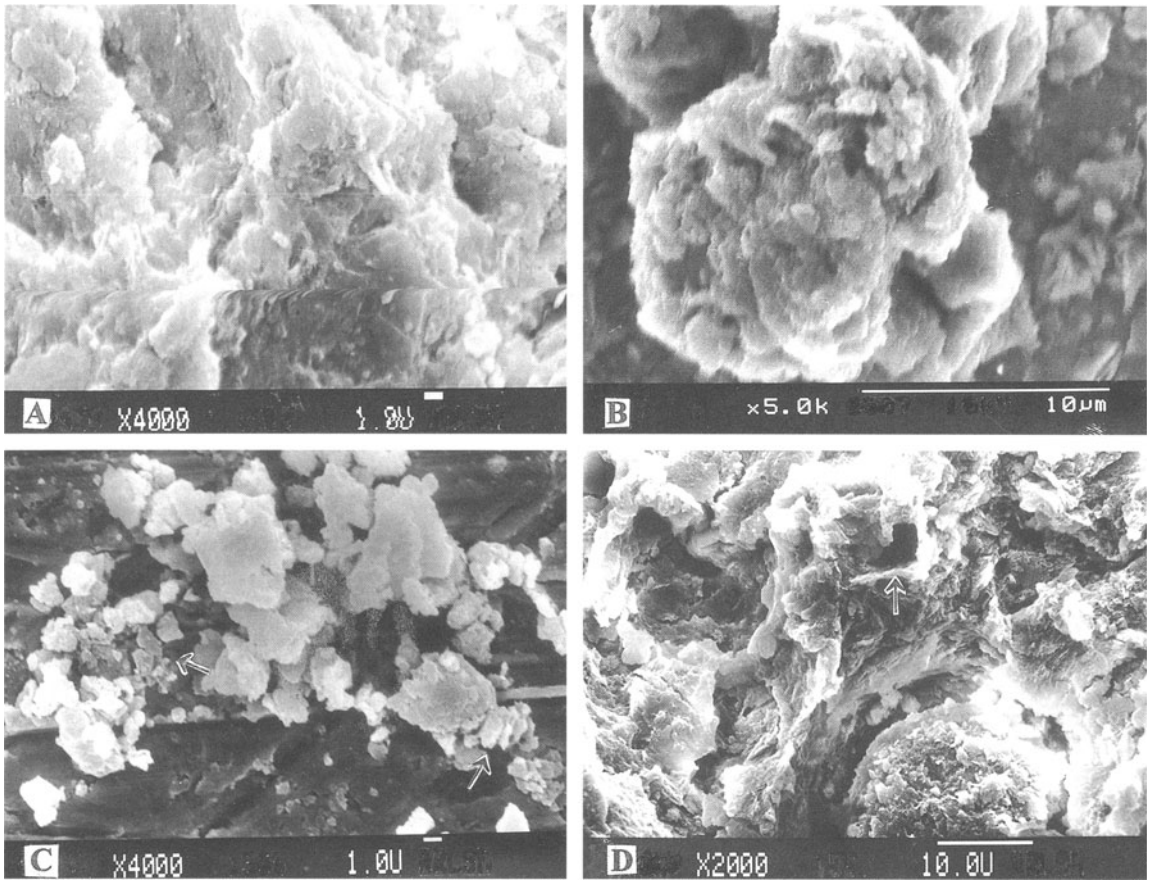

Figure 7. Scanning electron micrographs of sedimentary clays: (A) swirl texture with face-to-face arrangement of platy grains indicating the detrital origin of gray carbonaceous clay; (B) agglomeration of kaolinite by organic matter giving a flower-like appearance; (C) kaolinite of bimodal origin, face-to-face arrangement of fine platelets of kaolinite (arrow) surrounding larger ones, product of *in situ* crystallization from a water-laden environment; (D) plant remains from uppermost gray carbonaceous clay L15: kaolinite crystals, product of crystallization from Si -and-Al-rich solution and found to be intergrown in the etched pits of cubic Fe sulfide.

Al–Si-rich ionic solution within the microenvironment of plant fossils, thereby developing authigenic kaolinite. Simultaneously, dissolution of FeS_2 under oxidizing conditions, allows the percolation of acid-rich water through the available pore-structure and cavities within the clay. The iron released during dissolution precipitates as Fe oxyhydroxides. Microscopic examination of reddish yellow clay encircling the plant fossils in mottled L15 clay shows some minerals which are amorphous and with cornflake-like texture. This may be smectite, probably formed as a result of low leaching environment due to the precipitation of amorphous Fe oxyhydroxides (Figure 8A) during FeS_2 dissolution. The typical morphology of an Fe oxyhydroxide grain indicating *in situ* crystallization is shown in Figure 8B.

Hematite-rich clay. The microscopic examination of this clay shows the agglomeration of finer particles, by the cementing effect of hematite or amorphous Fe oxyhydroxides (Figure 9). In this genetic environment, the *in situ* kaolinization or the features of kaolinite recrystallization are absent. This is also evident from the FTIR patterns, where kaolinite shows a lower crystallinity.

This evidence indicates that the environmental conditions—oxidizing and reducing—have influenced the entire clay deposit. The oxidized weathering condition which led to the formation of hematite-rich clay, enhanced the dissolution of the FeS_2 present in the gray carbonaceous clay layers, creating a very acidic environment in which dissolution and reprecipitation of microcrystalline quartz and authigenic kaolinite occurred. In addition, the percolation of these SO_4^{2-} ions rendered the deposit more acidic resulting in the subsequent crystallization of FeS_2 in the microenvironment within the plant fossils in the residual white clay. The presence of overlying sedimentary deposits of the Warkallai Formation preserves the underlying residual

https://doi.org/10.1346/CCMN.2001.0490409 Published online by Cambridge University Press

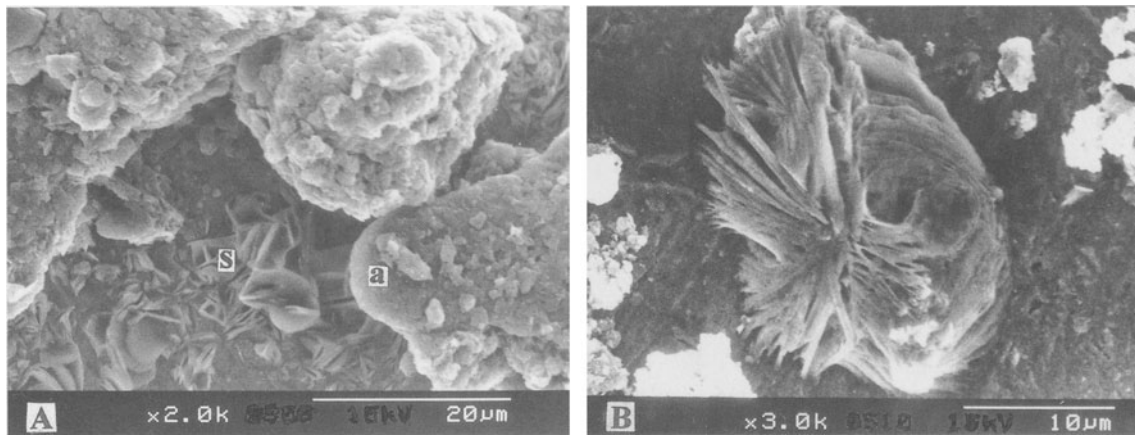

Figure 8. Scanning electron micrographs showing smectite and secondary iron oxides: (A) smectite precipitation (s) with cornflake-like texture and amorphous Fe hydroxides (a); (B) crystal of Fe oxyhydroxide showing *in situ* crystallization.

white clay deposit from intense post-Warkallai–pre-Quaternary lateritization.

Industrial application

Commercial evaluation of the representative sample collected from the residual white clay (L) is given in Table 3. This residual clay deposit shows a recovery of 46% (Table 3) for the <45 μm fraction. In this, the <2 μm fraction comprises 48%. Calcination of kaolinite prior to bleaching causes an enhancement in brightness of ~7.91 units compared to the crude clay. Correspondingly, the yellowness value also decreases by 1.57 units. Such an improvement indicates that the clay contains goethitic iron impurity (Kogel and Hall, 1999) which converts to hematite during calcination and is leached more efficiently. The pinkish-white fired color of the clay, even after bleaching, shows the presence of color-imparting impurities. Table 3 presents the properties of the fired samples as fired shrinkage, water adsorption, apparent porosity and bulk density. Increasing the sintering temperature to 800°C resulted in an increase in all the properties measured. Above this temperature, samples sintered at 1250°C exhibit increase in fired shrinkage (24.26%) and bulk density (0.81), with a corresponding reduction of apparent porosity (17.3%) and water adsorption (33.26%). This also results in a drastic increase in MOR of about ~235 kg/cm^2.

CONCLUSIONS

Our investigation indicates that the mineralogy, chemistry and morphology of the associated minerals

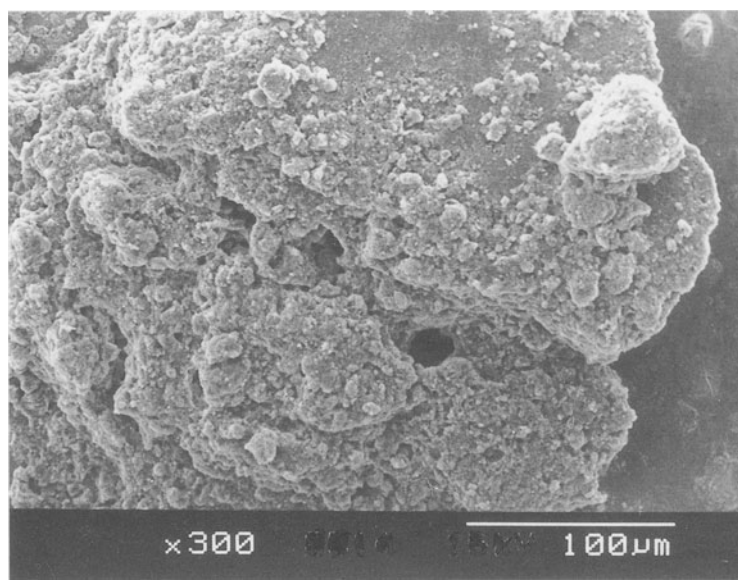

Figure 9. Agglomerated kaolinite platelets with amorphous iron oxide coating in hematite-rich clay.

https://doi.org/10.1346/CCMN.2001.0490409 Published online by Cambridge University Press

Table 3. Physical properties of china clay (<45 μm sample).

Clay recovery	46%
Raw color	Buff
Particle size distribution analysis:	
<2 μm	48%
<5 μm	72%
<10 μm	89%
<20 μm	99.5%
>20 μm	0.5%
Brightness/yellowness of raw clay	58.35/10.6%
Brightness/yellowness of calcined clay	62.32/11.02%
Brightness/yellowness after bleaching	59.48/10.9%
Brightness/yellowness after calcination and bleaching	66.26/9.35%
Viscosity	621 cps
Water of plasticity	40.2%
Dry linear shrinkage	3.9%
Green MOR	5.59 kg/cm^2
Fired properties	
Fired color (1250°C)	pinkish white
Fired linear shrinkage (1250°C)	16.08%
Fired MOR (1250°C)	235 kg/cm^2

	600°C	800°C	1000°C	1250°C
Fired volume shrinkage (%)	1.17	2.30	10.00	24.46
Water adsorption (%)	44.35	46.69	46.27	33.26
Apparent porosity (%)	22.40	23.35	23.13	17.3
Bulk density (g/cm^3)	0.66	0.65	0.69	0.81

in this deposit are closely related to the formation environment. The variation in kaolinite character in each layer as evident from XRD, DTA, IR, chemical analysis and SEM is related to the petrogenetic, stratigraphic and post-depositional conditions. It is found that kaolinite within the same deposit has itself been formed under three genetic environmental conditions: (1) oxidizing conditions for the detrital hematite-rich uppermost ferruginous clay follow on L16; (2) reducing environment for the deposition of FeS_2-enriched gray carbonaceous kaolinite seams L3 to L15; and (3) intense lateritized weathering conditions for the formation of the economically viable residual white clay L.

The structural and morphological studies indicate the recrystallization of kaolinite in the gray carbonaceous clays. Lower L3 clay showed textures characteristic of detrital and also *in situ* crystallization under water-laden conditions. *In situ* kaolinization into etched FeS_2 pits from Al-Si-enriched ionic solution occurs within the plant remains of the (L15) carbonaceous clay in an organic-enriched environment. Mineralization in plant remains in L1b indicates that this microenvironment does not favor the *in situ* kaolinite crystallization in the absence of an ample amount of organic chelators as in gray carbonaceous clay. The mineralogical assemblages such as pyrophyllite, muscovite with its typical fanning-out morphology with lenticular voids, and leached pits in pyrite crystals found within the plant remains from L1b indicate that kaolinization of this deposit is not yet complete. This is further proven by the fact that the concentration of trace elements is lowest for the residual clay L1a, which has undergone relatively less weathering. The sedimentary clay deposits of the Warkallai formation play a major role in protecting the underlying residual white clay from the ongoing lateritization.

Technological evaluation of this clay, which has a recovery rate of 46%, shows that this large deposit could be exploited commercially for use in the ceramics industry. A comparison of the specifications of this clay with ASTM indicates that this clay is suitable for white ware and sanitary ware applications.

ACKNOWLEDGMENTS

This research work is funded by the Council of Scientific and Industrial Research, India. The authors thank Robert J. Pruett and Jessica Elzea Kogel for their helpful comments during review of the manuscript. We also thank the Director, Regional Research Laboratory, Thiruvananthapuram, for providing the necessary facilities throughout this work.

REFERENCES

Al-Khalissi, F.Q. and Worrall, W.E. (1982) The effect of crystallinity on the quantitative determination of kaolinite. *Transactions of the British Ceramic Society,* **81,** 43–46.

Bennet, H. and Reed, R.A. (1971) *Chemical Methods of Silicate Analysis. A Handbook.* Academic Press, London, 272 pp.

Berner, R.A. (1984) Sedimentary pyrite formation: An update. *Geochimica et Cosmochimica Acta,* **48,** 605–615.

Brindley, G.W. (1986) Relation between structural disorder and other characteristics of kaolinite and dickites. *Clays and Clay Minerals,* **34,** 239–249.

Chen, P.-Y. Lin, M.-L. and Zheng, Z. (1997) On the origin of the name kaolin and the kaolin deposits of the Kauling and Dazhou areas, Kiangsi, China. *Applied Clay Science,* **12,** 1–25.

Farmer, V.C. (1979) Infrared spectroscopy. Pp. 285–337 in: *Data Handbook for Clay Minerals and other Non-metallic Minerals* (H. van Olphen and J.J. Fripiat, editors). Pergamon Press, New York.

Goldschmidt, V.M. (1958) *Geochemistry.* Oxford University Press, UK, 491 pp.

Gross, M.G (1971) Carbon determination. Pp. 573–596 in: *Procedure in Sedimentary Petrology.* (R.E. Carver, editor), Wiley Interscience, New York.

Heckroodt, R.O. and Buhmann, D. (1987) Genesis of South African residual kaolins from sedimentary rocks. Pp. 128–134 in: *Proceedings of the International Clay Conference, Denver, 1985.* (L.G. Schultz, H. van Olphen and F.A. Mumpton, editors). The Clay Minerals Society, Bloomington, Indiana.

Hinckley, D.N. (1963) Variability in "crystallinity" values among the kaolin deposits of the coastal plain of Georgia and South California. *Clays and Clay Minerals,* **11,** 229–235.

Keller, W.D. (1978) Classification of kaolins exemplified by their texture in Scan Electron Micrographs. *Clays and Clay Minerals,* **26,** 1–20.

Keller, W.D. (1985) The nascence of clay minerals. *Clays and Clay Minerals,* **33,** 161–172

Kogel, J.E., Hall, R.K. and Randy, K. (1999) *Process for improving the color and brightness of discolored goethite-containing materials.* United State Patent, 5,891,236.

Plançon, A., Giese, R.F., Snyder, R., Drits, V.A. and Bookin, A.S. (1989) Stacking faults in kaolin-group minerals: defect structures of kaolinite. *Clays and Clay Minerals,* **23,** 249–260.

Rajendran, C.P. and Narayanaswamy (1987) A note on the lateritization cycles associated with sedimentaries, Kasaragod district, Kerala. *Journal of Geological Society of India,* **30,** 309–314.

Rankama, K. and Sahama, T.H.G. (1952) *Geochemistry, 2nd edition.* University of Chicago Press, Chicago, 659 pp.

Robertson, I.D.M. and Eggleton, R.A. (1991) Weathering of granite muscovite to kaolinite and halloysite. *Clays and Clay Minerals,* **39,** 113–126.

Russell, J.D. (1987) Infrared methods. Pp. 133–173 in: *A Handbook of Determinative Methods in Clay Mineralogy.* (M.J. Wilson, editor). Chapman & Hall, London.

Schneider, J.W. and Schneider, K. (1990) Indirect method for the determination of pyrite in clays and shale after selective extraction with acid solutions. *Ceramic Bulletin,* **69,** 107–109.

Searle, A.B. and Grimshaw, R.W. (1960) *Chemistry and Physics of Clays.* Western Printing Services Ltd., Bristol, UK, 944 pp.

Stoch, L. and Sikora, W. (1976) Transformation of mica in the process of kaolinization of granites and gneisses. *Clays and Clay Minerals,* **24,** 156–162.

Vazquez, F.M. (1981) Formation of gibbsite in soil and saprolites of temperate-humid zones. *Clay Minerals,* **16,** 43–52.

White, G.N., Dixon, J.B., Weaver, R.M. and Kunkle, A.C. (1991) Genesis and morphology of iron sulfides in gray kaolins. *Clays and Clay Minerals,* **39,** 70–76.

E-mail of corresponding author: lali@csrrltrd.ren.nic.in

(Received 7 April 1999; revised 8 January 2001; Ms. 330; A.E. Jessica Elzea Kogel)